Effect of Simultaneous Addition of Three Sintering Aids: magnesium, lanthanum, and zirconium oxide on the Mechanical and optical properties of Alumina Ceramics fabricated by SPS Method

Amirhossein Karimi shargh
Malek Ashtar University of Technology
Mazaher Ramazani
Malek Ashtar University of Technology
Hossein Jamali
Malek Ashtar University of Technology
Fatemeh Davar
Davar@cc.iut.ac.ir

Isfahan University of Technology
Ehsan Mohammad Sharifi
Malek Ashtar University of Technology
Shahab Torkian
Malek Ashtar University of Technology
Alireza Nasr Esfahani
Malek Ashtar University of Technology

Article

Keywords: Alumina, triplex sintering aid, transparency, ceramics, SPS

Posted Date: April 4th, 2025

DOI: https://doi.org/10.21203/rs.3.rs-6268009/v1

Additional Declarations: No competing interests reported.

Version of Record: A version of this preprint was published at Scientific Reports on July 1st, 2025. See the published version at https://doi.org/10.1038/s41598-025-06197-1.

Abstract

This study investigates the synergistic effects of a novel triplex sintering aid system—magnesium oxide (MgO), lanthanum oxide (La_2O_3), and zirconium oxide (ZrO_2)—on the mechanical and optical properties of transparent alumina ceramics fabricated using spark plasma sintering (SPS). The specimens were sintered at 1350°C for 10 minutes under 70 MPa pressure. The sample with the highest zirconia content (sample Z: 100L100M300Z) achieved a bulk density of 3.94 g/cm^3, corresponding to 99.9% of the theoretical density of alumina. This sample exhibited an infrared transmission of 71.4% at 5 μm and a visible transmittance of 32% at 750 nm, surpassing values reported for single or dual sintering aid systems. Mechanical testing revealed a microhardness of 19.34 ± 0.1 GPa and a fracture toughness of 5.24 MPa.m$^{0.5}$ for sample Z. Additionally, this sample demonstrated the highest flexural strength of 356.83 MPa, attributed to its finer grain size, reduced porosity, and the synergistic effects of the triplex sintering aids. The results demonstrate a promising pathway for producing high-performance transparent alumina ceramics with tailored properties for demanding optical and mechanical applications.

1. Introduction

Alumina ceramics are highly valued for their exceptional mechanical properties, electrical insulation, and thermal stability, making them suitable for a wide range of industrial applications. Transparent alumina ceramics, in particular, are critical for use in armor, sensors, and advanced optical systems due to their impressive strength, thermal stability, and optical transparency. Alpha-alumina is a prominent material for infrared windows, offering 50–70% infrared transmission in the 3–5 μm wavelength range and excellent mechanical properties. However, its low impact resistance and fracture toughness remain significant limitations. These limitations can be addressed by optimizing sintering conditions to reduce temperature and time while maintaining a fine grain structure [1–5].

The performance of alumina ceramics can be significantly enhanced through the addition of appropriate sintering aids, particularly dual systems such as MgO-Y_2O_3, MgO-La_2O_3, or MgO-ZrO_2. These systems have been shown to improve density and mechanical properties in transparent alumina [3–5]. In this study, we investigate the combined effects of three sintering aids—magnesium oxide (MgO), lanthanum oxide (La_2O_3), and zirconium oxide (ZrO_2) —on the properties of alumina ceramics produced using the SPS method. Achieving high visible and infrared transparency in ceramics requires minimizing light scattering and ensuring that grain sizes are significantly smaller than the incident wavelength. Thus, achieving full density during sintering and preventing excessive grain growth are essential. The choice of sintering method is critical, and the SPS technique is particularly advantageous for producing materials with high density, short sintering times, and fine grain structures [6, 7].

In addition to sintering strategies, the use of sintering aids can inhibit grain growth, enhance density, and improve mechanical properties. However, the optimal amount of each additive must be carefully selected. Insufficient amounts may fail to achieve the desired optical properties, whereas excessive amounts can lead to porosity or secondary phase formation, thereby reducing transparency. For instance, Ge et al. demonstrated that 100 ppm La_2O_3 improves compactness and bulk density in alumina ceramics, reducing apparent porosity and enhancing mechanical properties [8]. Similarly, La^{3+} ions have been shown to curb grain growth, improving both infrared and visible transmission. However, increasing La_2O_3 concentration beyond 100 ppm does not further inhibit grain growth [8, 9].

Studies have also shown that triple additive systems, such as MgO-La_2O_3-Y_2O_3, enhance real in-line transmittance (RIT) compared to dual or additive-free systems. This improvement is attributed to the synergistic effects of the triple combination, with MgO playing a pivotal role by creating oxygen vacancies in the alumina structure, which facilitates the incorporation of Y and La atoms [10].

Apak et al. [11] investigated the effects of Y_2O_3 and MgO on the mechanical properties of alumina, producing transparent ceramics via SPS at 1300°C and 1340°C under 80 MPa pressure for 5 minutes. Their samples achieved densities ranging from 97.1–99.9%, and higher MgO concentrations (up to 300 ppm) resulted in increased density. Another study examined the influence of MgO on visible transmission at various sintering temperatures (1300, 1500, and 1700°C), finding that 300 ppm MgO at 1300°C yielded the highest transparency [12]. Additionally, zirconia additives have been shown to refine alumina grain structure, though concentrations above 300 ppm do not further enhance light transmission [9, 13].

While extensive research has explored the effects of single and dual sintering aids (e.g., MgO, La_2O_3, and ZrO_2) on the optical and mechanical properties of transparent alumina, no studies have comprehensively evaluated the simultaneous addition of MgO, La_2O_3, and ZrO_2 on the microstructure, light transmission, and the full suite of mechanical properties (e.g., hardness, fracture toughness, and flexural strength) of alumina. This study aims to address this gap by investigating the synergistic effects of a triple sintering aid system on the properties of SPS-processed alumina ceramics.

2. Experimental

2.1. Synthesis of Precursors and Sintered Samples

In this study, α-alumina powder with a particle size of 200 nm and high purity (99.9%) was purchased from US Research Nanomaterials Inc. The chemical precipitation process for the sintering aids involved using magnesium nitrate ($Mg(NO_3)_2$), lanthanum nitrate ($La(NO_3)_3$), and zirconium chloride ($ZrOCl_2$) salts, all sourced from Merck, Germany. Initially, a slurry was prepared by dispersing 2.2 g of nanosized alumina in 50 mL of deionized water. Subsequently, magnesium nitrate, lanthanum nitrate, and zirconium oxychloride were added according to the compositions specified in Table 1. By adding ammonia and adjusting the pH to 9.5, hydroxide ions (Mg^{2+}, La^{3+}, Zr^{4+}) were precipitated onto the suspended alumina particles. The resulting slurry was dried in an oven at 60°C for 8 hours, followed by calcination at 800°C to convert the hydroxides ($Mg(OH)_2$, $La(OH)_3$, and $Zr(OH)_4$) into their corresponding metal oxides (MgO, La_2O_3, and ZrO_2.

Table 1
Composition, sample codes, and Archimedes density of samples prepared with different amounts of sintering aids.

$ZrOCl_2.8H_2O$ (g)	$Mg(NO_3)_2.6H_2O$ (g)	$La(NO_3)_3.6H_2O$ (g)	Relative density (%)	ppm of sintering aid	Sample code
0.0002	0.00127	0.0005	98.7	100MgO-100La_2O_3-50ZrO_2	G: 100M-100L-50Z
.0002	0.0025	0.0005	97.1	200 MgO – 100 La_2O_3-50 ZrO_2	H: 200M -100 L-50 Z
.00005	0.00127	0.0005	98.7	100 MgO – 100 La_2O_3-100 ZrO_2	X: 100M -100 L-100Z
.0005	0.0025	0.0005	99.1	200 MgO – 100 La_2O_3-100 ZrO_2	Y: 200M -100L-100Z
0.00156	0.00156	0.0005	99.9	100 MgO – 100 La_2O_3-300 ZrO_2	Z: 100 M -100 L-300 Z
-	0.00127	-	96.1	100 MgO	100M
-	0.00127	0.0005	97.9	100 MgO – 100 La_2O_3	100M100L
0.00156	0.00127	0.0005	98.1	100 MgO – 300 ZrO_2	100M300Z

Sample consolidation was performed using a spark plasma sintering (SPS) machine (manufactured by MUT University, Iran) at a temperature of 1350°C, with a heating rate of 50°C/min, under a pressure of 70 MPa for 10 minutes. Graphite molds with a diameter of 2 cm were used for the sintering process.

2.2. Characterization Techniques

X-ray diffractometry (XRD): Performed using an X’Pert Pro MPD device (Panalytical, Netherlands) with a copper X-ray tube (wavelength: 1.542 Å), operating at 40 kV and 25 mA. The step size was set to 0.03 degrees.

Field emission scanning electron microscopy (FESEM): Structural investigations were performed using an FEI model (USA).

Density measurements: Evaluated using Archimedes’ method.

Visible-ultraviolet (UV-Vis) transmission tests: Conducted over a wavelength range of 200–800 nm using a Ray Leigh UV-1600 device.

Infrared (IR) transmission tests: Investigated using Infralum FT-08 LUMEX infrared spectroscopy.

Three-point bending tests: Performed using a Hounsfield H25KS (England) equipped with a 500 N load cell, moving at a speed of 0.1 mm/min.

Microhardness testing: Conducted using a 101/642-MiTi model (Mitutoyo, Japan) by applying a 1 kg load for 10 seconds.

3. Results and Discussion

3.1. Structural and Phase Analysis

The X-ray diffraction (XRD) pattern of the initial alumina powder is presented in Fig. 1. The diffraction peaks correspond to α-alumina (JCPDS card no. 01-073-1512), with lattice parameters of a = 0.47544 nm and c = 1.297 nm, confirming a rhombohedral crystal structure. Using the Williamson-Hall method, the crystallite size of the alumina powder was calculated to be 43.4 nm.

The XRD patterns of the bulk samples with different sintering aid compositions, after SPS treatment at 1350°C are shown in Fig. 2. Due to the detection limit of XRD (phases below 5 wt.% are not detectable), all samples exhibited diffraction patterns consistent with the α-alumina phase, with no evidence of additional or decomposed phases.

3.2. Microstructural Analysis

Scanning electron microscopy (SEM) images of the α-alumina powder with the three sintering aids (MgO, La_2O_3, and ZrO_2) are presented in Fig. 3. The images reveal alumina nanoparticles with sizes ranging from 200 to 250 nm, alongside smaller particles (< 100 nm) attributed to the precipitated sintering aids after calcination at 800°C.

Energy-dispersive X-ray spectroscopy (EDS) analysis of the samples with compositions 100M100L300Z and 100M100L50Z is shown in Fig. 4. The EDS results indicate that the weight percentages of lanthanum, magnesium, and zirconium exceeded the theoretical values due to fluorescence errors inherent in the EDS analysis.

3.3. Density and Microstructure

The bulk density of all samples, as evaluated by Archimedes' method, is summarized in Table 1. The results show that the 100M-100L-300Z (Z) sample, with the highest zirconia content (300 ppm), achieved the highest bulk density of 3.94 g/cm³, corresponding to 99.9% of the theoretical density of α-alumina. This improvement is attributed to the role of zirconia in reducing surface tension and grain boundary energy, thereby enhancing the sintering process and promoting denser microstructures [8, 9, 14–18].

The high bulk density (3.94 g/cm³) achieved in the 100M100L300Z sample is a direct result of the combined effects of the triple sintering aids. The addition of ZrO_2 reduces surface tension and grain boundary energy, promoting densification during the sintering process [9, 13]. Meanwhile, MgO and La_2O_3 stabilize the microstructure and prevent the formation of pores, further enhancing the density of the material [8–11]. The ability to achieve near-theoretical density in such a short sintering time is a testament to the effectiveness of the triplex sintering aid system, as it allows for the production of high-performance transparent alumina ceramics with minimal defects.

Field emission scanning electron microscopy (FESEM) images of the fracture surfaces of the prepared samples are shown in Fig. 5. The 100M-100L-300Z (Z) sample exhibited the smallest grain size and no observable porosity, confirming its superior densification.

The microstructure of the 100M100L300Z sample, characterized by its fine grain size and lack of observable porosity, is a direct result of the synergistic effects of the triple sintering aids. The addition of ZrO_2 inhibits grain growth through its phase transformation mechanism, while MgO and La_2O_3 stabilize the grain boundaries and prevent the formation of secondary phases. This combination of effects results in a dense, uniform microstructure that is essential for achieving both high optical transparency and mechanical strength. The ability to control grain size and porosity through the use of multiple sintering aids is a key advantage of the triplex system, as it allows for the development of materials with tailored properties for specific applications.

3.4. Elemental Distribution

X-ray mapping of the elemental distribution in the Z sample is presented in Fig. 6. The analysis confirms the uniform distribution of Zr, La, and Mg throughout the alumina grains, indicating the effective incorporation of the sintering aids. The uniform distribution of Zr, La, and Mg is crucial for achieving consistent and predictable material properties. The absence of clustering or segregation suggests that the chemical precipitation method effectively dispersed the sintering aids throughout the alumina grains. This uniform dispersion likely contributes to the enhanced densification and grain growth control observed in the subsequent analyses.

3.5. UV-Vis and IR spectra and microstructures

The transmission curves for the prepared samples in the visible and infrared ranges are shown in Fig. 7. The 100M-100L-300Z (Z) sample exhibited the highest visible transmittance of 32% at 750 nm and the highest infrared transmittance of 71.4% at 5 μm.

Figure 8 shows photographic images of the sintered samples, demonstrating the visible transparency of the Z and Y samples, as evidenced by the clear visibility of the text "Al_2O_3" placed behind the samples.

A comparison of the optical results of this study with other reported works is provided in Table 2. The infrared transmittance achieved in this work is higher than that of alumina prepared with single sintering aids (e.g., MgO or La_2O_3) or triple sintering aids (e.g., MgO, ZrO_2, and Y_2O_3) [12, 15, 16].

Table 2
Comparison of the optical transmittance of this study with other reported works.

Visible transmission (at λ = 750 nm)	IR transmission (at λ = 5 μm)	T/P	Sintering aid content	Ref.
35	67	1500°C/ 50 MPa	450 MgO – 450Y_2O_3-450ZrO_2	[15]
-	42	1500°C /80MPa	500 ppm MgO	[12]
20	65	1500°C /70MPa	100 ppm MgO-100 ppm La_2O_3	[16]
32	71.4	1350°C /70MPa	100 MgO – 100 La_2O_3-300 ZrO_2	Current work

Figure S1 (Supporting Information File 1) shows the visible light transmission spectra of the samples with different sintering aid compositions. The sample without sintering aids exhibited no transmission in the visible region. In contrast, samples containing 100 ppm magnesia (100M), 100 ppm magnesia + 100 ppm lanthanum oxide (100M100L), and 100 ppm magnesia + 300 ppm zirconium oxide (100M300Z) showed transmission values of 7%, 14%, and 23%, respectively, at a wavelength of 700 nm. Notably, the sample containing all three sintering aids—100 ppm magnesia, 100 ppm lanthanum oxide, and 300 ppm zirconium oxide (100M100L300Z)—achieved a transmission value of 29% at 700 nm. These results highlight the critical role of the triple sintering aid system in enhancing the optical transparency of alumina ceramics.

Figure S2 (Supporting Information File 1) presents cross-sectional field emission scanning electron microscopy (FESEM) images of alumina disks with varying sintering aid compositions. Key observations include:

1. Without sintering aids: The alumina grain size grew to 10 μm, with significant intergranular porosity (indicated by arrows).
2. With 100 ppm magnesia (100M): A mixture of coarse grains (10 μm) and finer grains (50 nm) was observed.
3. With 100 ppm magnesia + 100 ppm lanthanum oxide (100M100L): The grain size decreased to 4–5 μm.
4. With 100 ppm magnesia + 300 ppm zirconium oxide (100M300Z): The grain size further decreased to 3 μm.

The number of pores (indicated by arrows) decreased significantly from Figure S2a to S2d, demonstrating the effectiveness of sintering aids in reducing porosity and refining grain structure.

3.6.Mechanical Properties: Microhardness, Fracture Toughness and Flexural Strength

The microhardness of the samples was calculated using Eq. 1:

(1) $H = 0.1891 \times \frac{P}{2(a^2)}$

where:

- H = hardness (GPa),
- P = applied load (N),
- a = radius of the indentation (mm).

The results, presented in Table 3, show that the 100M100L300Z (Z) sample exhibited the highest microhardness. For fracture toughness, Eq. 2 was used:

Table 3
Hardness and micro-hardness values of the sintered samples.

Hardness (GPa)	Microhardness (GPa)	Sample code
018.56 ± 0.3	19.36 ± 0.2	G: 100M-100L-50Z
18.01 ± 0.5	18.18 ± 0.5	H: 200M -100L-50 Z
16.97 ± 0.2	16.6 ± 0.2	X:100M-100L-100Z
17.51 ± 0.1	17.16 ± 0.1	Y: 200M -100L-100Z
19.34 ± 0.2	19.14 ± 0.1	Z: 100 M -100 L-300 Z

(2) $K_{IC} = K\left(\frac{E}{H}\right)^{\frac{1}{2}}\left(\frac{P}{c^{\frac{3}{2}}}\right)$

where:

- KIC = fracture toughness (MPa·$m^{0.5}$),
- K = dimensionless constant (0.0264) [18],
- E = elastic modulus (GPa),
- P = applied load (N),
- c = crack length (mm).

The results, summarized in Table 4, demonstrate that the 100M100L300Z (Z) sample achieved the highest fracture toughness. The significant improvement in fracture toughness observed in the 100M100L300Z sample can be attributed to the combined effects of the triple sintering aids. ZrO_2, in particular, plays a key role in enhancing fracture toughness through its phase transformation mechanism, which induces compressive stresses that hinder crack propagation. Additionally, the presence of MgO and La_2O_3 at the grain boundaries stabilizes the microstructure and reduces the likelihood of intergranular fracture. This multi-mechanism approach to improving fracture toughness is a key advantage of the triplex sintering aid system, as it allows for the development of transparent alumina ceramics with both high optical transparency and excellent mechanical performance.

Table 4
Fracture toughness values of the sintered samples.

K_{IC} (MPa.m$^{0.5}$)	C (µm)	Sample code
1.48	192.25	G: 100M-100L-50Z
3.29	114.5	X:100M-100L-100Z
3.81	102.5	Y: 200M -100L-100Z
5.24	84	Z: 100 M -100 L-300 Z

3.6.1.Flexural Strength

The three-point bending strength of the samples was calculated using Eq. 3:

(3) $$\sigma = \frac{8PL}{\pi D^3}$$

where:

- σ = flexural strength (MPa),
- P = breaking force (N),
- L = distance between supports (mm),
- D = sample diameter (mm).

The results, presented in Table 5 and Fig. 9, show that the 100M100L300Z (Z) sample exhibited the highest flexural strength. This improvement is attributed to the reduction in grain size, lower porosity, and the synergistic effects of the triple sintering aids.

Table 5
Flexural strength and grain size values of the sintered samples.Table 6: Comparison of the properties of this work with other reported studies.

Flexural strength (MPa)	Grain size (μm)	Sample code
269	5	G: 100M-100L-50Z
195	2.5	H: 200M -100L-50 Z
220	2	X:100M-100L-100Z
188	2	Y: 200M -100L-100Z
356	2	Z: 100 M -100 L-300 Z

The mechanical properties of the 100M100L300Z sample, including its high hardness (19.34 GPa) and flexural strength (356.83 MPa), are a direct result of the synergistic effects of the triple sintering aids. The fine grain size achieved through the addition of ZrO_2, combined with the grain boundary strengthening effects of MgO and La_2O_3, results in a material with superior resistance to deformation and fracture. The reduction in porosity and the uniform distribution of the sintering aids further contribute to the enhanced mechanical performance, making this material suitable for applications requiring both high strength and optical clarity.

3.7.Role of Sintering Aids in Transparency and Density

The high relative density achieved in the 100M100L300Z (Z) sample corresponds to a reduction in porosity, which is crucial for improving transparency. High porosity levels lead to light scattering due to the significant difference in refractive indices between air ($n \approx 1$) and alumina ($n \approx 1.76$). This scattering results in the darkening of the ceramic.

The addition of zirconia (ZrO_2) plays a key role in grain refinement. As shown in Table 1 and the SEM images, increasing the zirconium salt content reduces grain size of alumina. This effect is attributed to the tetragonal-to-monoclinic phase transformation of zirconia, which induces a 3–5% volume expansion and inhibits grain growth at alumina grain boundaries [9, 18].

Furthermore, magnesia (MgO) promotes the formation of a stable $MgAl_2O_4$ spinel phase at grain boundaries, which also prevents alumina grain growth [1–5, 21–24]. The inclusion of lanthanum oxide (La_2O_3) stabilizes the spinel network, further enhancing the microstructure. The synergistic effect of the triple sintering aid system significantly improves the transparency and mechanical properties of alumina.

The observed improvements in transparency and mechanical properties can be attributed to several factors. The combination of MgO, La_2O_3, and ZrO_2 creates a multi-faceted approach to controlling grain boundary mobility and defect formation. MgO promotes the formation of $MgAl_2O_4$ spinel, which not only inhibits grain growth but also scavenges impurities. La_2O_3 stabilizes the spinel structure and reduces oxygen vacancies, while ZrO_2's phase transformation induces compressive stresses that hinder crack propagation. The synergy between these three sintering aids results in a material with a refined microstructure, reduced porosity, and enhanced resistance to mechanical failure.

The high transparency achieved in this study is particularly noteworthy. The combination of high density and fine grain size minimizes light scattering, allowing for efficient transmission of both visible and infrared radiation. This makes the material suitable for applications where optical clarity and mechanical robustness are essential. Furthermore, the enhanced mechanical properties, such as hardness, fracture toughness, and flexural strength, expand the range of potential applications to include demanding environments where resistance to wear, impact, and high stress is critical.

The enhanced optical transparency observed in the 100M100L300Z sample can be further explained by the interplay between grain size reduction and porosity minimization. The addition of ZrO_2, in particular, plays a critical role in refining the grain structure, as the tetragonal-to-monoclinic phase transformation induces compressive stresses that inhibit grain growth. This, combined with the stabilizing effect of La_2O_3 on the spinel network and the grain boundary pinning effect of MgO, results in a microstructure with minimal light scattering centers. The uniform distribution of these sintering aids, as confirmed by X-ray mapping, ensures that the material maintains high transparency across both visible and infrared wavelengths. This multi-faceted approach to controlling microstructure is key to achieving the high transmittance values reported in this study.

3.8.Comparison with Previous Studies

The fracture toughness of the 100M100L300Z (Z) sample (5.24 $MPa \cdot m^{0.5}$, Table 6) is superior to values reported for alumina with single or dual sintering aids (e.g., 4.4 $MPa \cdot m^{0.5}$ for MgO-Y_2O_3 [18] and 2.5–3.52 $MPa \cdot m^{0.5}$ for pure alumina [19–21]). Similarly, the flexural strength of the Z sample (356.83 MPa) exceeds that of alumina with 0.5 wt.% MgO (322 MPa) [24]. These results demonstrate the superiority of the triple sintering aid system in enhancing both mechanical and optical properties.

Table 6

Parameter	Current work	[12]	[16]	[15]	[3]
Additives	**100 ppm MgO, 100 ppm La_2O_3, 300 ppm ZrO_2**	**500 ppm MgO**	**100 ppm MgO-100 ppm La_2O_3**	450 MgO – 450Y_2O_3-450ZrO_2	**100 ppm MgO, 400 ppm Y_2O_3**
Fracture Toughness (MPa√m)	**5.24**	**4.8**	**5.1**	**4.9**	**-**
Flexural Strength (MPa)	**356**	**320**	**340**	**310**	**193**
Visible Light Transmission (700 nm, %)	**32**	**28**	**30**	**25**	**13**
Infrared Transmission (5 μm, %)	**71.4**	**61**	**67**	**68**	**60**
Synthesis Method	**(SPS)**	**(SPS)**	**(SPS)**	**(SPS)**	**(SPS)**

The results of this study not only demonstrate the superiority of the triplex sintering aid system but also highlight the potential for further optimization. For instance, the fracture toughness of 5.24 $MPa \cdot m^{0.5}$ achieved in this work is significantly higher than that reported in previous studies using single or dual sintering aids. This improvement can be attributed to the synergistic effects of MgO, La_2O_3, and ZrO_2, which collectively enhance grain boundary strength and reduce crack propagation. Furthermore, the flexural strength of 356.83 MPa surpasses that of alumina with 0.5 wt.% MgO (322 MPa) [24], indicating that the combination of these three sintering aids not only improves optical properties but also significantly enhances mechanical performance. These findings suggest that the triplex sintering aid system could be a promising approach for developing high-performance transparent alumina ceramics for demanding applications such as armor and optical windows.

4. Conclusion

In this study, the effects of three sintering aids—magnesia (MgO), lanthanum oxide (La_2O_3), and zirconia (ZrO_2)—on the optical and mechanical properties of transparent alumina ceramics were investigated. The 100M100L300Z (Z) sample, containing 100 ppm MgO, 100 ppm La_2O_3, and 300 ppm ZrO_2, exhibited the highest infrared transmittance (71.4% at 5 μm) and visible transmittance (32% at 750 nm). This sample also demonstrated superior mechanical properties, including a hardness of 19.34 GPa, fracture toughness of 5.24 $MPa \cdot m^{0.5}$, and flexural strength of 356.83 MPa. These improvements are attributed to the synergistic effects of the triple sintering aids, which reduce grain size, minimize porosity, and increase densification.

The optical properties of the 100M100L300Z sample, particularly its high infrared transmittance (71.4% at 5 μm) and visible transmittance (32% at 750 nm), are a direct result of the combined effects of the triple sintering aids. The reduction in grain size and porosity minimizes light scattering, while the uniform distribution of the sintering aids ensures that the material maintains high transparency across a wide range of wavelengths. The ability to achieve such high levels of transparency while maintaining excellent mechanical properties is a significant advancement in the field of transparent ceramics, opening up new possibilities for applications in optical systems.

Declarations

Conflict of Interest

The authors declare that they have no conflict of interest with any individual, company, or organization concerning this research.

Author statement:

A.K., M.R., H. J, EM. S, S. T, AN.E and F.D. wrote the main manuscript text and prepared figures. All authors reviewed and edited the manuscript. All authors contributed in interpretation and data gathering and editing manuscript.

Acknowledgement

Data availability:The datasets used and/or analysed during the current study available from the corresponding author on reasonable request.

Data Availability

“The datasets used and/or analysed during the current study available from the corresponding author on reasonable request.”

References

1. Akinribide, Ojo Jeremiah, Gadifele Nicolene Mekgwe, Samuel Olukayode Akinwamide, Fehmi Gamaoun, Chamil Abeykoon, Oluwagbenga T. Johnson, and Peter Apata Olubambi. "A review on optical properties and application of transparent ceramics." *journal of materials research and technology* 21 (2022): 712-738.
2. Yin, Jun, Xiao Li, Xi Zhang, Shengquan Yu, and Yuanming Lai. "Progress in sintering technology of transparent polycrystalline alumina ceramics." *Journal of Advanced Dielectrics* 14, no. 06 (2024):

2330002.

3. Gao, Huiliang, Hussein Humedy Chlib Alkaaby, Safa K. Hachim, Holya A. Lafta, Musaddak Maher Abdul Zahra, Zainab Sabri Abbas, Munthir Mohammed Radhy AL Kubaisy et al. "Investigation of mechanical properties and transparency of spark plasma sintered Mg^{2+} and Y^{3+} codoped α-Al_2O_3 nanoparticles synthesized via coprecipitation." *Journal of Materials Research and Technology* 23 (2023): 1052-1061.
4. Park, CheolWoo, Elisa Torresani, Chris Haines, Darold Martin, and Eugene A. Olevsky. "Transparent Al2O3 fabricated by energy efficient spark plasma sintering." *Journal of Materials Science* 58, no. 29 (2023): 11872-11885.
5. Kuang, Zhong, Ming Yin, Zhuoying Jia, Xiaoqiang Li, and Shengquan Yu. "The preparation of highly transparent alumina ceramics with excellent mechanical performance via co-doping strategy." *Journal of Alloys and Compounds* (2025): 179497.
6. Shahriari, Masoumeh, Mohammad Reza Loghman Estarki, Hojatollah Mansouri, Hossein Jamali, and Mehran Sardarian. "The effect of size and type of alumina nanopowder phase on the transparency and bending strength of bodies sintered with MgO and La2O3 sintering aid." *Journal of the Australian Ceramic Society* 59, no. 4 (2023): 1079-1093.
7. Akinribide, Ojo Jeremiah, Gadifele Nicolene Mekgwe, Samuel Olukayode Akinwamide, Fehmi Gamaoun, Chamil Abeykoon, Oluwagbenga T. Johnson, and Peter Apata Olubambi. "A review on optical properties and application of transparent ceramics." *journal of materials research and technology* 21 (2022): 712-738.
8. Ge, Xing Ze, Qi Ge, Xing Shuo Ge, Deng Hui Ji, Ying Huang, Zhong Lun Zhang, and Hong Bo Zhang. "Influence of La2O3 Addition on Microstructure and Mechanical Properties of Al2O3 Ceramics." In *Materials Science Forum*, vol. 956, pp. 69-77. Trans Tech Publications Ltd, 2019.
9. Lallemant, Lucile, Nicolas Roussel, Gilbert Fantozzi, Vincent Garnier, Guillaume Bonnefont, Thierry Douillard, Bernard Durand et al. "Effect of amount of doping agent on sintering, microstructure and optical properties of Zr-and La-doped alumina sintered by SPS." *Journal of the European Ceramic Society* 34, no. 5 (2014): 1279-1288.
10. Roussel, Nicolas, Lucile Lallemant, Bernard Durand, Sophie Guillemet, Jean-Yves Chane Ching, Gilbert Fantozzi, Vincent Garnier, and Guillaume Bonnefont. "Effects of the nature of the doping salt and of the thermal pre-treatment and sintering temperature on Spark Plasma Sintering of transparent alumina." *Ceramics International* 37, no. 8 (2011): 3565-3573.
11. Apak, Burcu, G. Göller, Yücel Onüralp, and Filiz Çinar Şahin. "The effects of codoping Y2O3 on MgO doped spark plasma sintered Al2O3." *Advances in Science and Technology* 63 (2011): 74-78.
12. Shahbazi, H., M. Tataei, M. H. Enayati, A. Shafeiey, and M. Azizi Malekabadi. "Structure-transmittance relationship in transparent ceramics." *Journal of Alloys and Compounds* 785 (2019): 260-285.
13. Tyagi, Jyoti, Sanjeev Kumar Mishra, and Shahzad Ahmad. "Transparent ceramics: The material of next generation." In *Metal Oxides for Next-Generation Optoelectronic, Photonic, and Photovoltaic Applications*, pp. 45-75. Elsevier, 2024.

14. Oparina, I. B., and A. G. Kolmakov. "Methods for obtaining transparent polycrystalline ceramics from aluminum oxide." *Refractories and Industrial Ceramics* 62 (2021): 196-201.
15. Stuer, Michael, Zhe Zhao, Ulrich Aschauer, and Paul Bowen. "Transparent polycrystalline alumina using spark plasma sintering: effect of Mg, Y and La doping." *Journal of the European Ceramic Society* 30, no. 6 (2010): 1335-1343.
16. Shahriari, M., H. Jamali, H. Mansouri, M. R. Loghman Estarki, and M. Sardarian. "Fabrication of Spark Plasma Sintered Spark Plasma Sintered Transparent Alumina Using Magnesium Oxide and Lanthanum Oxide as Sintering-Assisted." *Journal of Advanced Materials in Engineering (Esteghlal)* 41, no. 3 (2022): 31-40.
17. Apak, Burcu, Halide Esra Kanbur, Esra Ozkan Zayim, Gultekin Goller, Onuralp Yucel, and Filiz Cinar Sahin. "Transparent Polycrystalline Alumina Obtained by SPS: Single and Double Doping Effect." *Supplemental Proceedings: Materials Processing and Interfaces* 1 (2012): 481-487.
18. Boldin, M. S., A. A. Popov, A. A. Murashov, N. V. Sakharov, S. V. Shotin, A. V. Nokhrin, V. N. Chuvil'deev, N. Yu Tabachkova, and K. E. Smetanina. "Investigation of the effect of a small addition of ZrO2 on the density and growth of grains of fine-grained aluminum oxide." *Technical Physics* 67, no. 7 (2022): 570-580.
19. Ratzker, Barak, Avital Wagner, Sergey Kalabukhov, and Nachum Frage. "Improved alumina transparency achieved by high-pressure spark plasma sintering of commercial powder." *Ceramics International* 46, no. 13 (2020): 21794-21799.
20. Kuang, Zhong, Ming Yin, Zhuoying Jia, Xiaoqiang Li, and Shengquan Yu. "The preparation of highly transparent alumina ceramics with excellent mechanical performance via co-doping strategy." *Journal of Alloys and Compounds* (2025): 179497.
21. Pristinskiy, Yuri, Nestor Washington Solis Pinargote, and Anton Smirnov. "The effect of MgO addition on the microstructure and mechanical properties of alumina ceramic obtained by spark plasma sintering." *Materials today: proceedings* 19 (2019): 1990-1993.
22. Harris, Daniel C. *Materials for infrared windows and domes: properties and performance*. Vol. 158. SPIE press, 1999.
23. Zhang, Luping, Quan Liu, Dazhao Yu, Mi Lu, and Jianping Lin. "Effect of sintering process on the properties of transparent Al2O3." *Materials Science and Technology* 39, no. 8 (2023): 926-932.
24. Ratzker B, Wagner A, Sokol M, Kalabukhov S, Dariel MP, Frage N. Optical and mechanical properties of transparent alumina fabricated by high-pressure spark plasma sintering. Journal of the European Ceramic Society. 2019 Jul 1;39(8):2712-9.

Figures

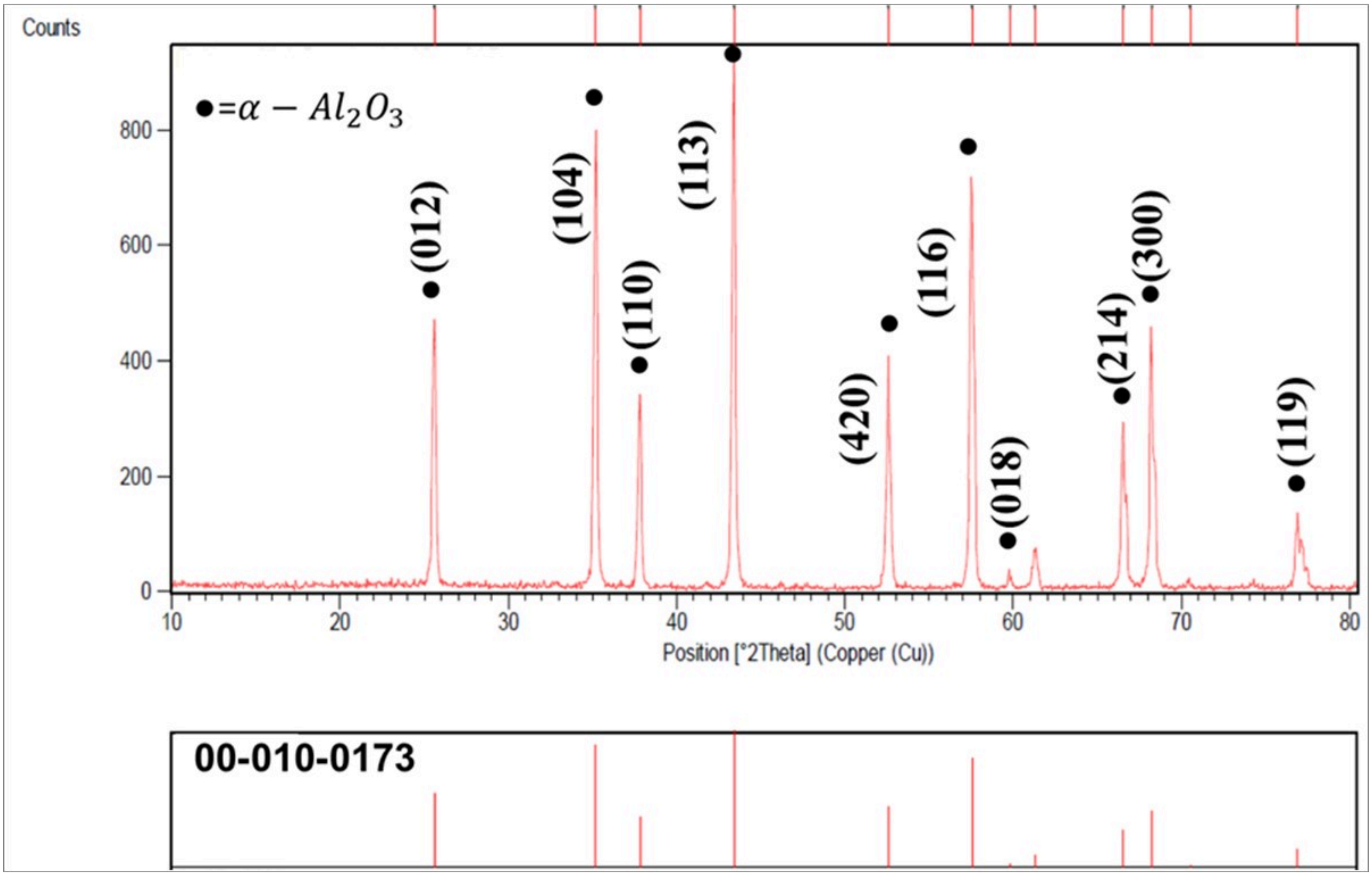

Figure 1

X-ray diffraction (XRD) pattern of the as-purchased alumina powder.

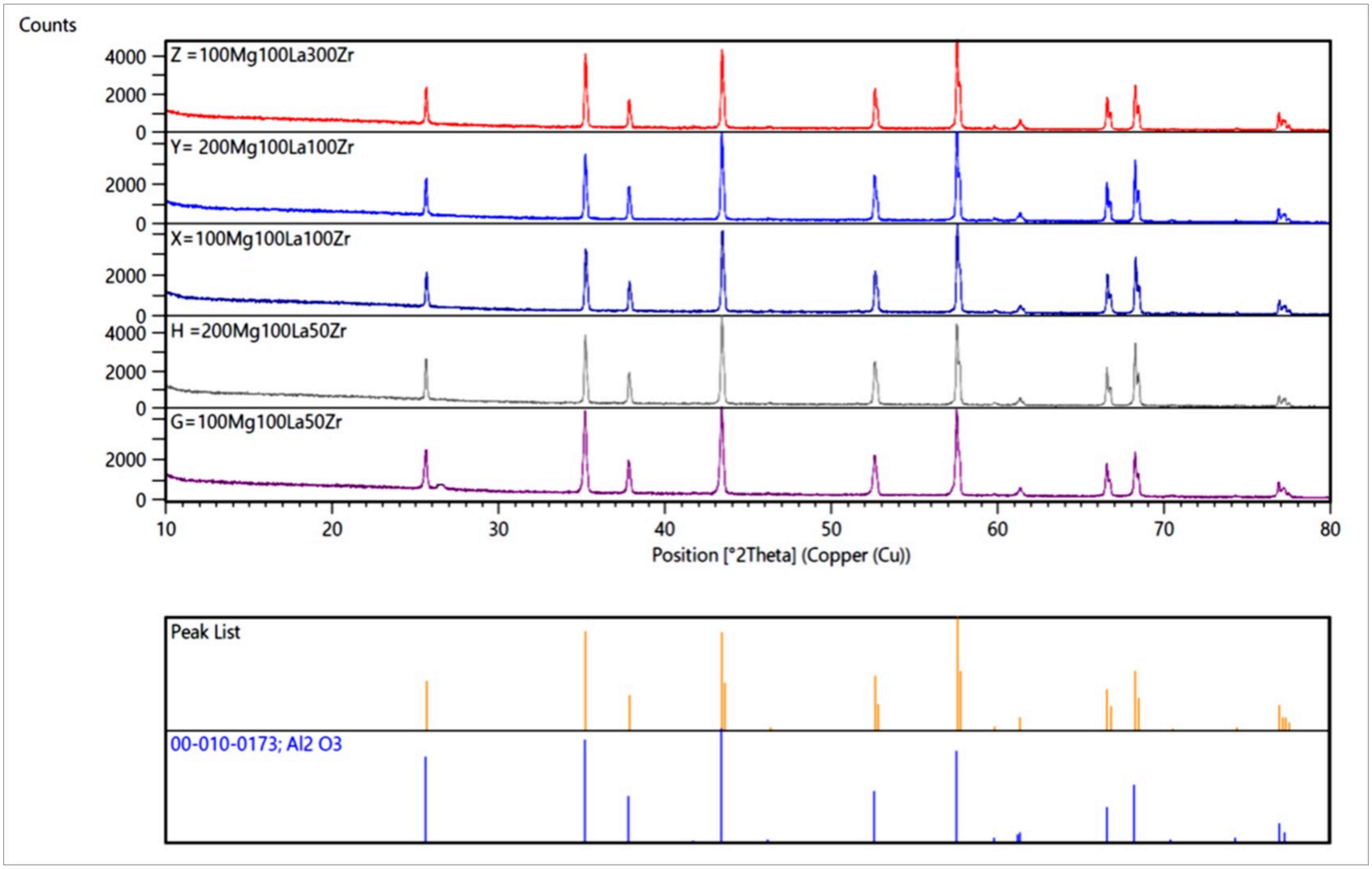

Figure 2

X-ray diffraction (XRD) patterns of consolidated alumina powders with different amounts of sintering aids.

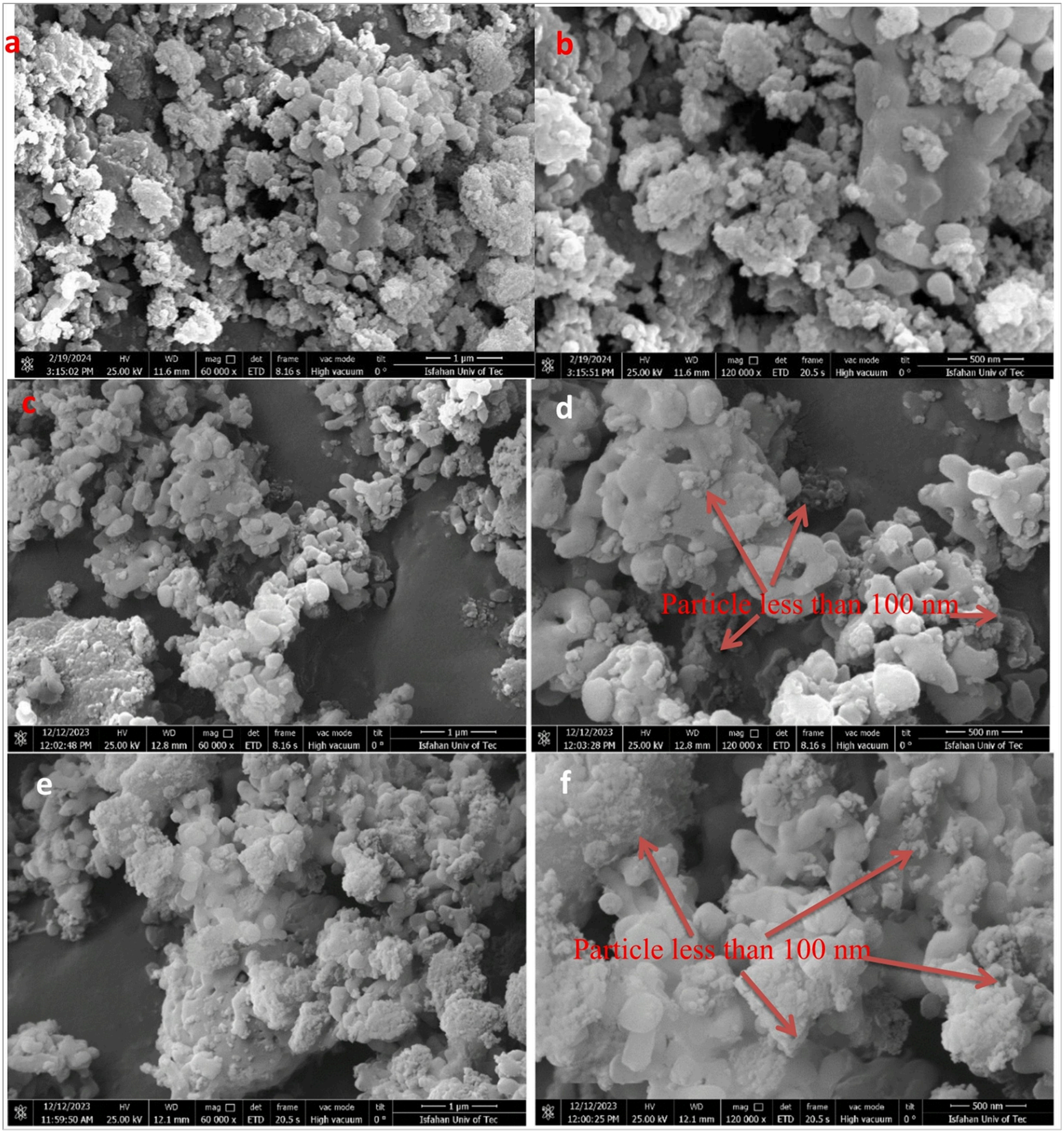

Figure 3

Scanning electron microscopy (SEM) images of the powders: (a, b) pure alumina; (c, d) G sample (50Z100L-100M); (e, f) Z sample (300Z100L-100M).

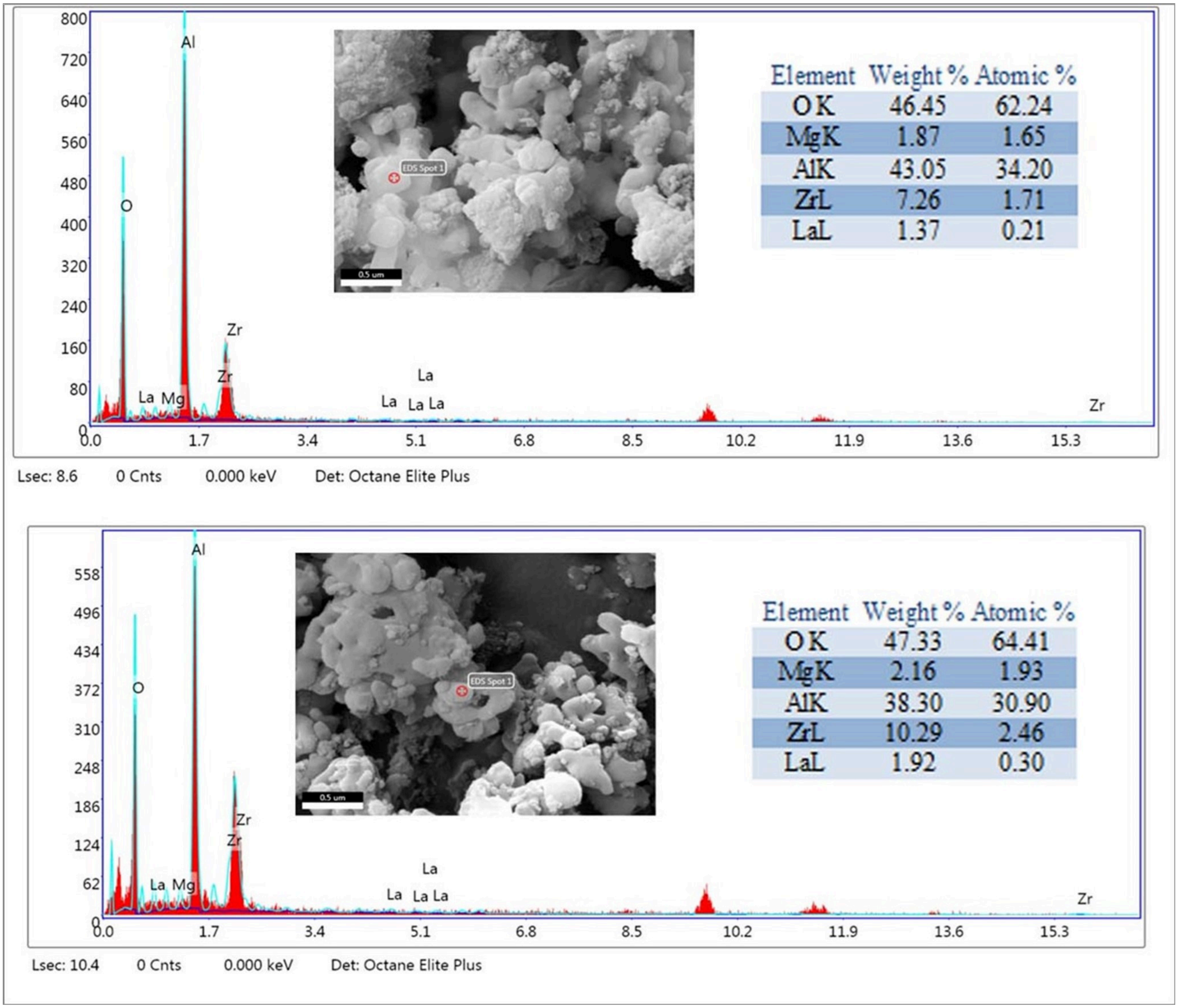

Figure 4

Cross-sectional field-emission scanning electron microscopy (FESEM) images of samples with different amounts of sintering aids.

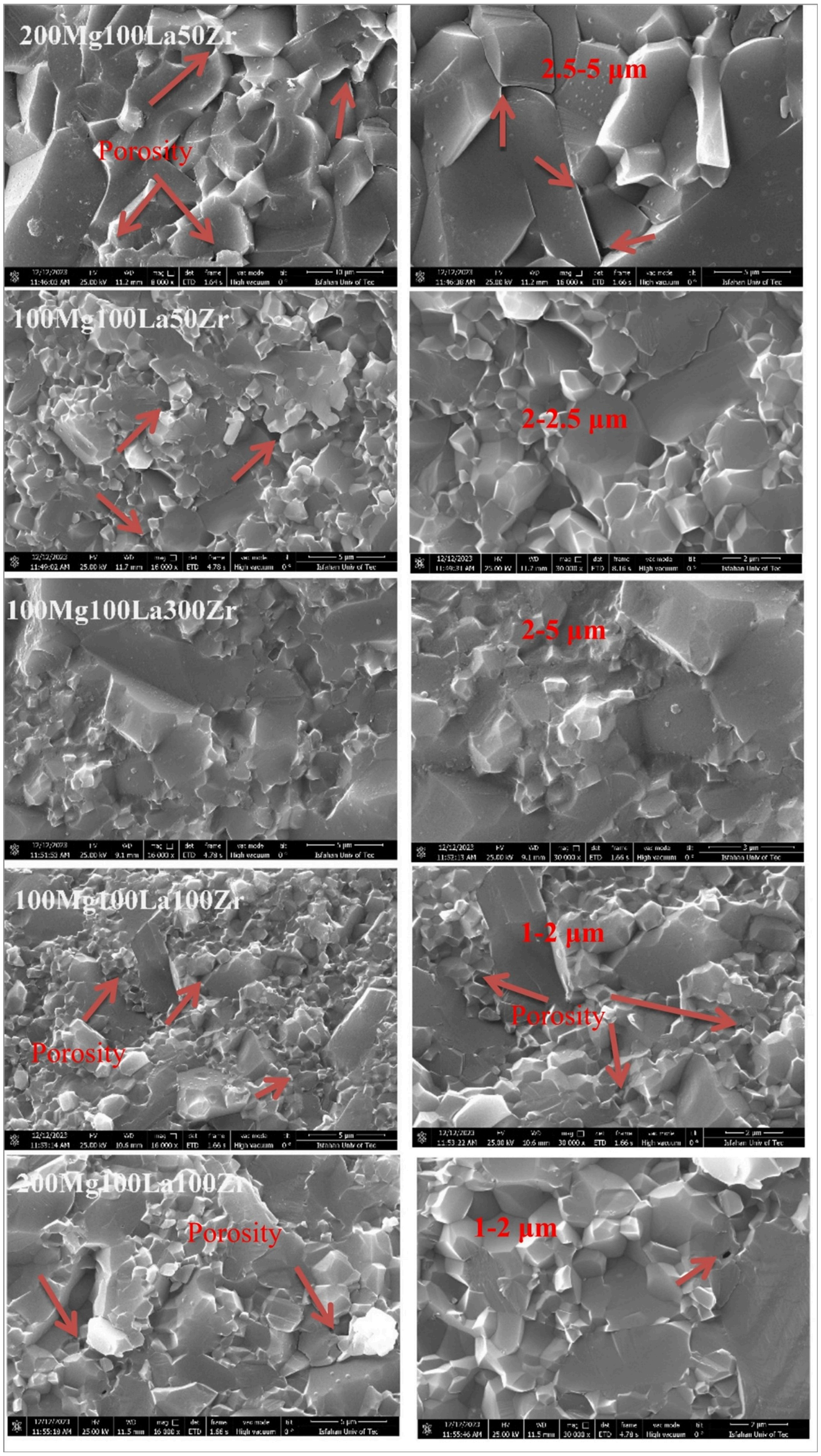

Figure 5

Fracture cross-section images of samples with different amounts of sintering aids.

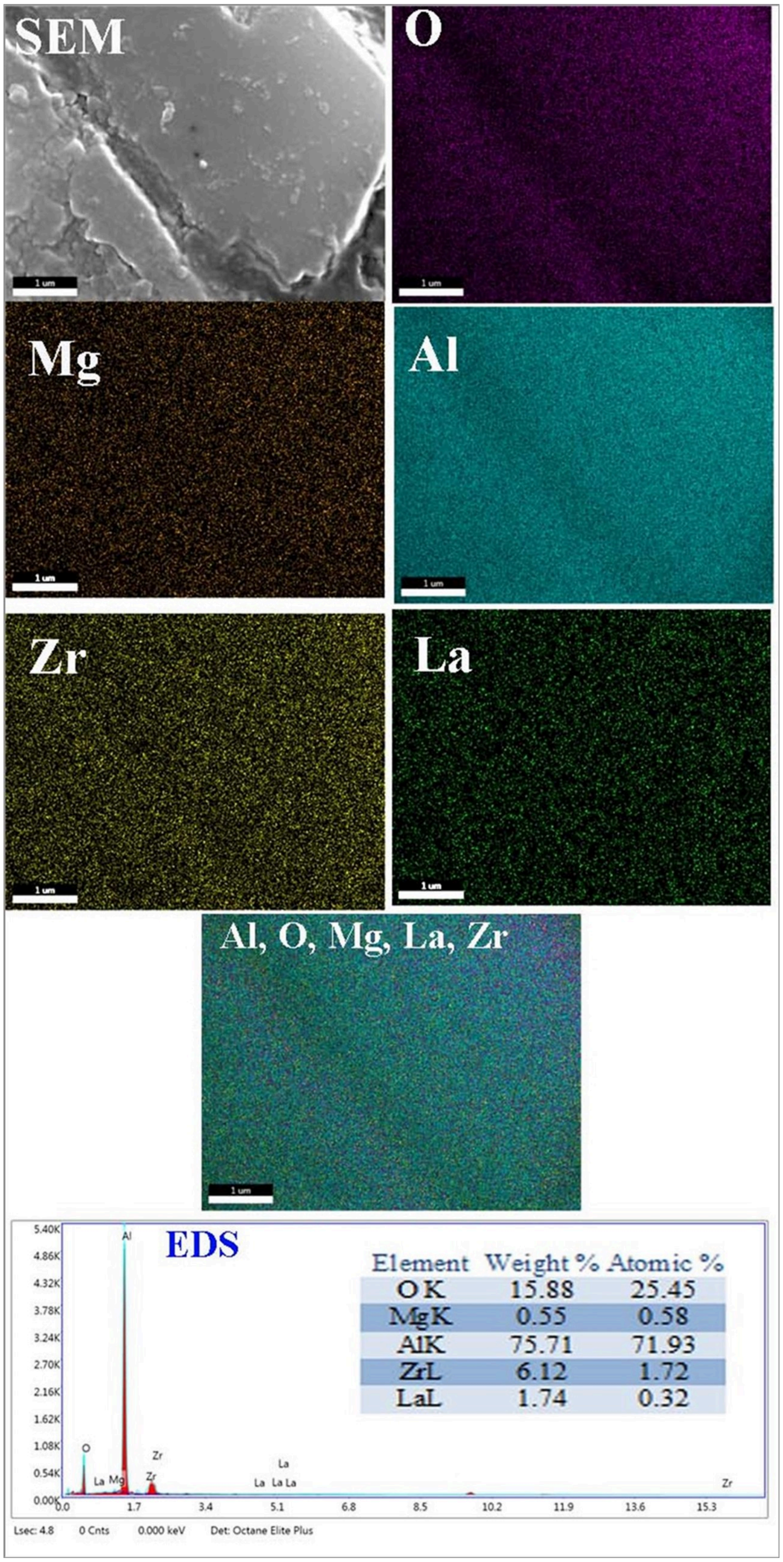

Figure 6

Energy-dispersive X-ray spectroscopy (EDS) mapping showing the distribution of elements, along with EDS analysis of bulk alumina containing three sintering aids—magnesia, lanthanum oxide, and zirconia—for sample code Z.

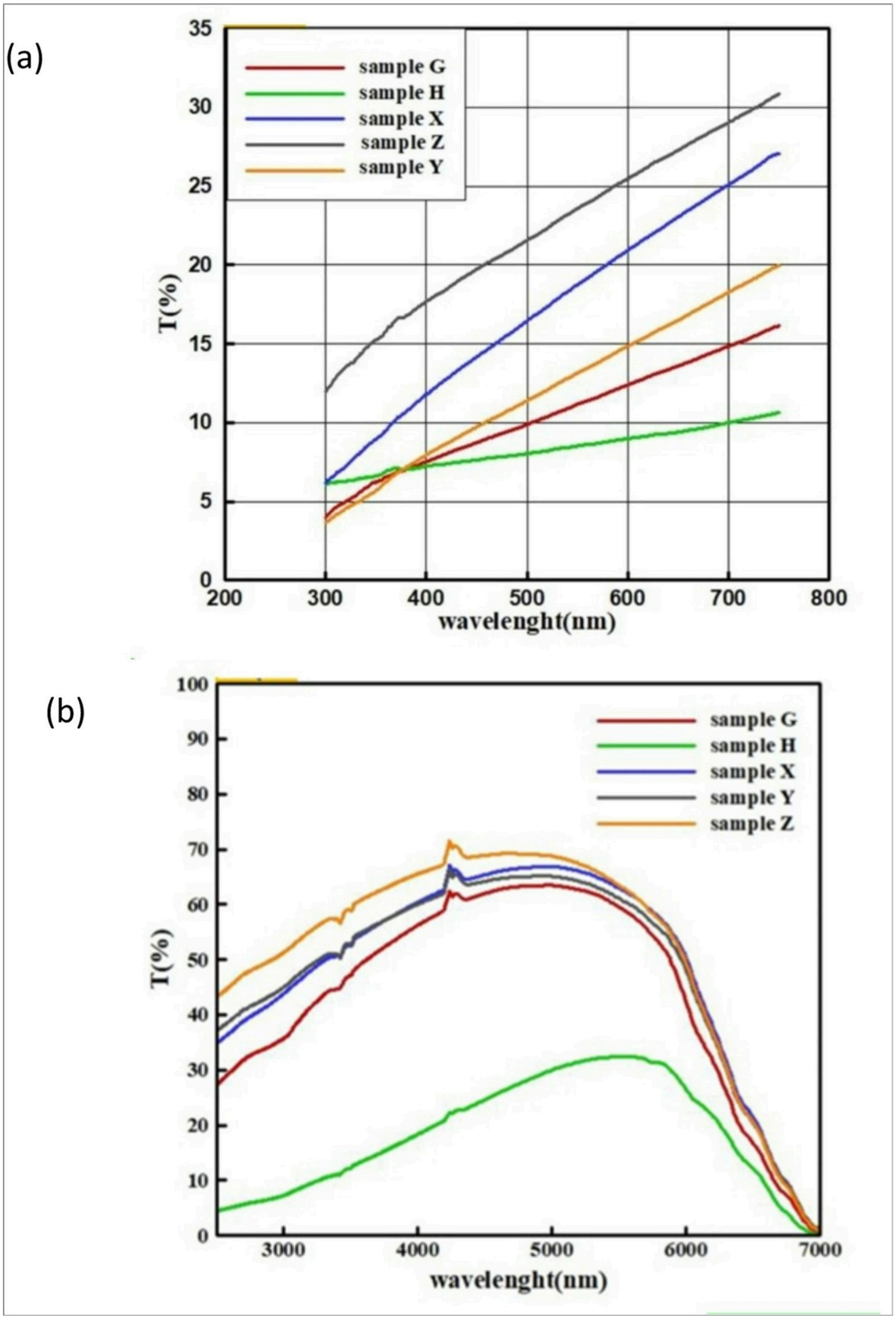

Figure 7

Images of sintered samples with different amounts of sintering aids.

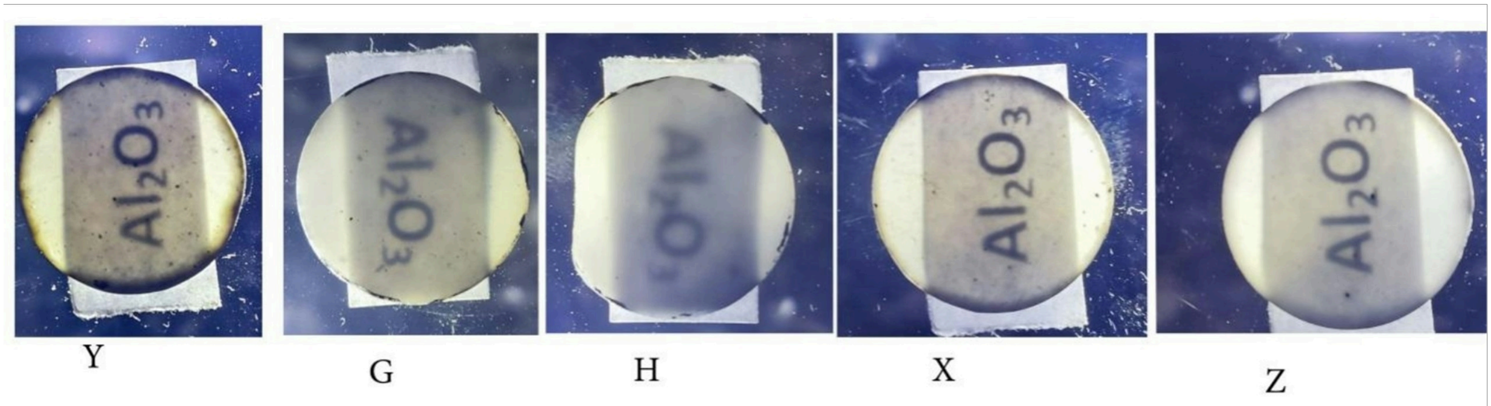

Figure 8

Flexural strength test results: (A) Stress-strain diagram of the samples.

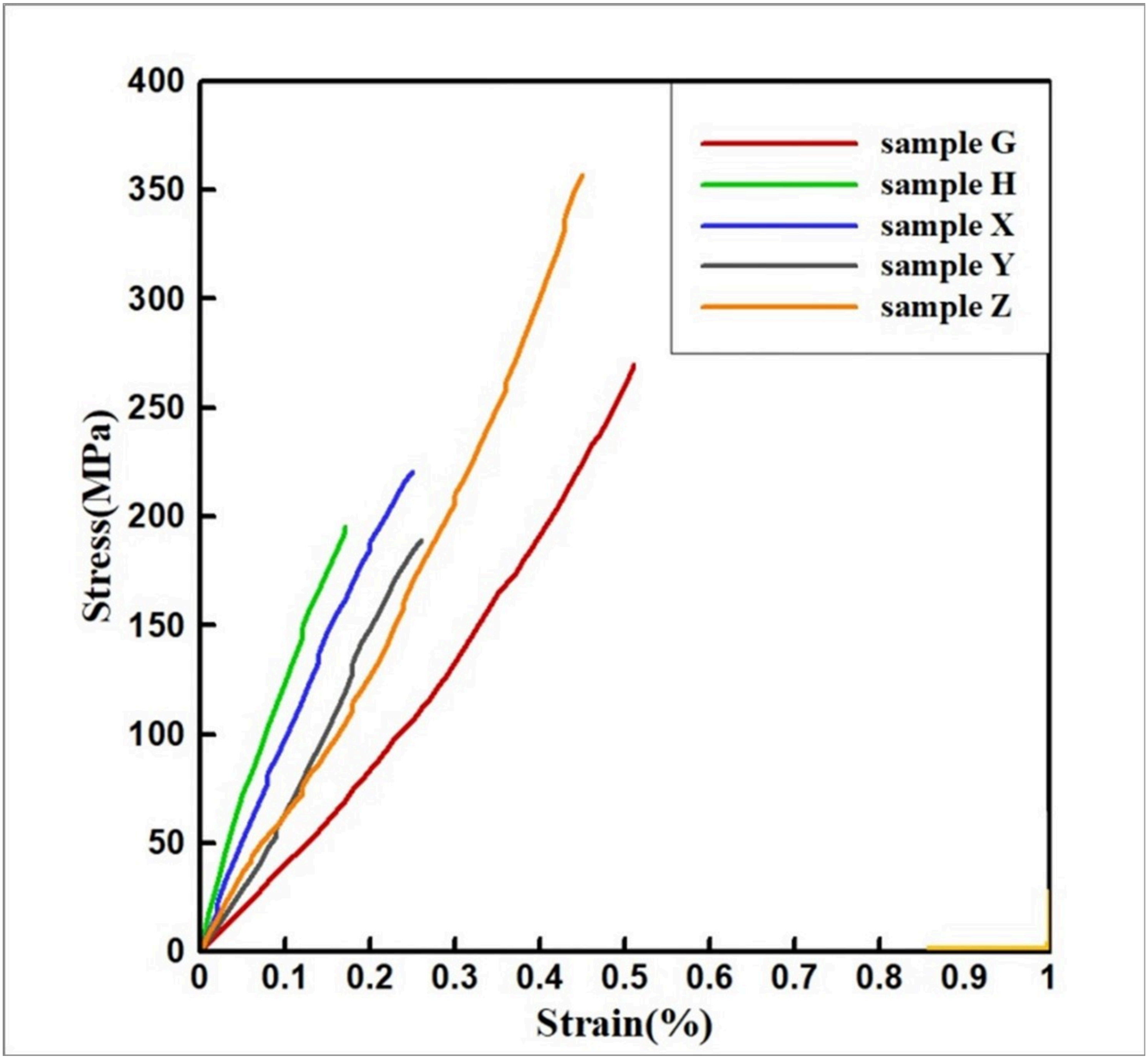

Figure 9

Flexural strength test results: (A) Stress-strain diagram of the samples.

Supplementary Files

This is a list of supplementary files associated with this preprint. Click to download.

- mFigsupport20121402Copy.docx